Journal of the Brazilian Society of Mechanical Sciences and Engineering (2023) 45:46
https://doi.org/10.1007/s40430-022-03958-1

TECHNICAL PAPER

Material and geometric nonlinear buckling of simply supported columns

Joon Kyu Lee[1] · Byoung Koo Lee[2] · Dai Soon Ahn[3] · Gweon Sik Kim[2]

Received: 2 August 2022 / Accepted: 6 December 2022 / Published online: 28 December 2022

Abstract
This study investigated the material and geometric nonlinear buckling of simply supported columns. The column body material followed Ludwick's constitutive law. Rectangular and elliptical cross sections were considered, and corresponding generalized moments of inertia (GMIs) were explicitly formulated. By applying the GMIs, the governing differential equations and boundary conditions of post-buckling columns were derived based on the Bernoulli–Euler beam theory, and the buckling loads and elastica were computed using numerical methods. To derive the elastica of buckling columns, the differential equations were integrated using the Runge–Kutta method, and the eigenvalues of the buckling load were determined using the bisection method. In our numerical experiments, the GMI formulae were applied, and parametric studies were conducted to analyze post-buckling columns in terms of buckling load, equilibrium path, elastica, and nonlinear stress along the cross section.

Keywords Generalized moment of inertia · Material and geometric nonlinear · Ludwick constitutive law · Column · Buckling · Elastica

1 Introduction

Recently, nonlinear elastic materials have been used as major structural members to support external compressive loads stably [1]. Ludwick-type materials are a family of representative nonlinear materials that follow a load-strain relationship of $\sigma = E\varepsilon^{1/n}$, where (ε, σ) denote the strain and stress, respectively, n is the material constant, and E is the modulus of elasticity [2]. The relationship $\sigma = E\varepsilon^{1/n}$, which is called the Ludwick constitutive law, can be used to calculate the bending moment $M = EI_g\kappa^{1/n}$, where I_g is the generalized moment of inertia (GMI) and κ is the curvature caused by M. It is important to formulate I_g in advance for buckling analysis, which is the main focus of this study.

Over the past few decades, calculation methods for GMI I_g have only been formulated by researchers for three cross-sectional planar areas. Lee [3] calculated I_g as $I_g = [0.5^{(1+1/n)}n/(2n+1)]ab^{(2+1/n)}$ for a rectangular cross section with width a and height b. Brojan and Kosel [4] computed I_g for a superellipsoidal cross section using a beta function that is explicitly expressed in an integral form. Lee and Lee [5] developed a calculation method for I_g for regular polygonal cross sections, where I_g was explicitly formulated using an integral formula. Five types of regular polygonal cross sections, namely triangles, squares, pentagons, hexagons, and circles, were considered as numerical examples. Kim et al. [6] formulated I_g for an elliptical cross section with semi-axes a and b based on the results of Brojan and Kosel [7], which was expressed in terms of the area A, but not the semi-axes a and b. Beyond the cross-sectional shapes mentioned above, additional formulas for I_g have not yet been derived.

Regarding geometric nonlinear analysis, the first study focusing on elastica was conducted by Euler [8], where thin rods of linear elastic materials were investigated. Following the study by Euler, both linear elastic materials and

Technical Editor: João Marciano Laredo dos Reis.

✉ Byoung Koo Lee
bkleest@wku.ac.kr

[1] Department of Civil Engineering, University of Seoul, Dongdaemun-Gu, Seoul 02504, Korea

[2] Department of Civil and Environmental Engineering, Wonkwang University, Iksan-Si 54538, Jellabuk-Do, Korea

[3] Bumhan Construction Corp., Jeonju-Si 54966, Jellabuk-Do, Korea

nonlinear elastic materials were considered for elastica analyses. Additionally, several elastica problems related to geometric and material nonlinearities have been investigated. We now review representative studies that have analyzed the deformed elastica related to our study.

First, regarding geometrical nonlinear elastica problems for linear materials, elastica studies similar to Euler's classical work are reviewed. Such studies include analyses of the large deflection of Euler beams using Bernoulli–Euler beam theory by Bisshopp and Drucker [9]; largely deformed elastica of Timoshenko beam-columns with internal joints, where the non-conservative loads were considered by Aristizabal-Ochoa [10]; shear deformable maximum column strength with constant volume and regular polygonal cross sections by Lee and Lee [11]; finite deflection of elastic rods following a hyperbolic tangent law by Oden and Childs [12]; large deflection of tapered cantilever beams considering distributed loads, concentrated loads, and tip coupling by Lee et al. [13]; Euler buckling loads with the corresponding buckled elastica of a non-prismatic column with a constant volume by Lee and Oh [14]; and bifurcation elastica of a slender beam subjected to axial external thrust by Berkey and Freedman [15]. Second, regarding nonlinear materials, several studies addressing elastica behavior have been conducted. For example, Giardina and Wei [16] and Anatolyevich and Yokovlevna [17] conducted two representative studies, where a material hardened by plastic deformation according to the Ramberg–Osgood constitutive law was considered.

In bending analysis, the material and geometric nonlinear behavior of structural members should be considered based on the GMI I_g. In the literature, I_g has been applied to elastica analysis, which considers highly deformed geometric nonlinear beams/columns. We now review the most representative works on beams/columns made of the Ludwick-type materials considered in this study. Lewis and Monasa [2] studied a largely deformed cantilever beam and applied coupling to the free end, where the exact curvature of the deformed beam was considered. Lee [3] applied the shear force formula to derive differential equations for the elastica of a buckled cantilever beam. Lee and Lee [5] studied post-buckling elastica for regular polygonal nonlinear cantilever columns made of Ludwick-type materials. Kim et al. [6] computed the buckling load and buckled elastica of nonlinear cantilever columns with elliptical cross sections that which followed the Ludwick constitutive law. Brojan and Kosel [7] applied the relationship between strain and stress to a superellipsoidal cross section. Eren [18] studied cantilever beam elastica with a uniform load and vertical point load. Eren [19] calculated simple beam elastica with a uniform load as a function of curvature expressed by arc length functions of two different types. Jung and Kang [20] studied the deformed elastica of uniform rectangular columns composed of nonlinear fibrous materials subjected to horizontal and vertical point loads. Saetiew and Chucheepsakul [21] derived first-order simultaneous differential equations to compute the buckling load of a linearly tapered column. Brojan and Kosel [7] investigated the stability of Euler columns considering their buckled shapes. Borboni and Santis [22] investigated cantilever beams with asymmetrical cross sections subjected to nonlinear bending under vertical and horizontal point loads with moment coupling. Liu et al. [23] studied curved beam elastica considering the effects of axial expansion, which implicitly formulated the corresponding stress–strain relationships.

As discussed above, the subject of the GMI I_g and nonlinear column buckling remains an important topic in classical mechanics. In the case of nonlinear column buckling, the conventional moment of inertia of a plane area I, which only applies to linear materials, is no longer valid for nonlinear members that follow the Ludwick constitutive law [3, 4]. Therefore, it is necessary to develop I_g formulations for various cross-sectional shapes and apply I_g to the buckling analysis of appropriate structural members for real-world engineering. From this perspective, this study has two main goals: reformulating I_g in a manner that is applicable to nonlinear elastic column buckling and applying I_g to the buckled column problem.

In this study, the GMIs for regular elliptical as well as rectangular cross section were formulated analytically and explicitly, and when applied to cantilever beam elastica, a uniformly distributed load was considered. The results for the stress and strain imposed on the cross section along the depth of the section, which are some of the most important design criteria for material and geometric nonlinear columns in actual engineering, are presented based on numerical experiments.

We begin by reformulating I_g for rectangular and elliptical cross sections based on theories from the literature [3–5]. This includes the derivation of governing differential equations with corresponding boundary conditions for buckled column elastica with a simply supported end and the development of numerical solution methods. Finally, based on numerical experiments, parametric studies of the GMI I_g and elastica of buckled columns are conducted and discussed extensively.

Our elastic analysis is based on the following assumptions: no initial imperfections exist in the column axis, the column material is inextensible/incompressible, and the plane of the cross section remains flat, even after buckling.

2 GMI for Ludwick-type material cross sections

2.1 Configuration of cross sections

Prior to buckling analysis, for columns following the Ludwick constitutive law, the calculation method for I_g

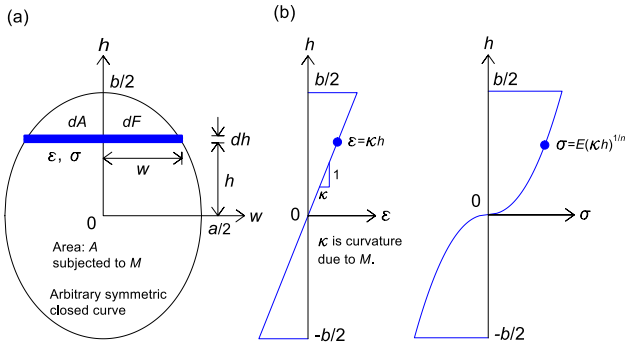

Fig. 1 **a** Symmetrical cross section acted to M and **b** stress ε and strain σ distributed along depth of cross section

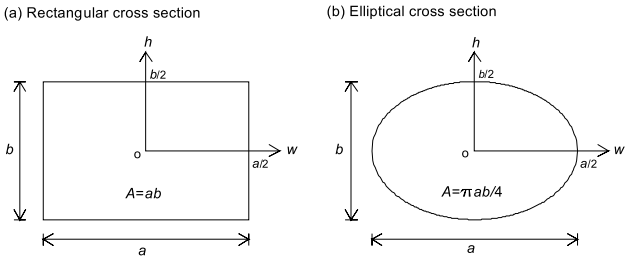

Fig. 2 Configuration of **a** rectangular and **b** elliptical cross section

is summarized based on theory from the open literature [3–5] and reformulated for the rectangular and elliptical cross sections considered in this study. Formulating I_g for a nonlinear elastic column is an essential preprocessing step.

Figure 1a presents an arbitrary planar cross section symmetrical about the w and h axes, where an elliptical area with semi-axes of $a/2$ and $b/2$ is presented as an example. The bending moment M is applied to the cross section through which the strain ε is linearly distributed and the stress σ for a nonlinear material is nonlinearly distributed along the cross-sectional depth h, as shown in Fig. 2b, where n is the material constant and E is the Young's modulus.

For Ludwick-type materials, the relationship between $\sigma-\varepsilon$ and the curvature κ is given as follows [24]:

$$\varepsilon = \kappa h, \tag{1}$$

$$\sigma = E\varepsilon^{1/n} = E(\kappa h)^{1/n} \tag{2}$$

The infinitesimal force $\mathrm{d}F$ on an area $\mathrm{d}A$ at the coordinate h can be obtained as

$$\mathrm{d}F = \sigma \mathrm{d}A = E(\kappa h)^{1/n} w dh, \tag{3}$$

where w is a function of h (i.e., $w = f(h)$) for any closed curve along the cross-sectional boundary.

The bending moment M imposed on area A can be obtained using Eq. 3 as

$$M = \int \mathrm{d}M = \int (\mathrm{d}F)h = E\kappa^{1/n} \int_{-b/2}^{b/2} w h^{1+1/n} \mathrm{d}h = EI_g \kappa^{1/n}, \tag{4}$$

where the GMI I_g is defined as

$$I_g = \int_{-b/2}^{b/2} w h^{1+1/n} \mathrm{d}h \tag{5}$$

Note that if $n = 1$ (i.e., linear elastic material), then I_g is reduced to $I_g = I$, which is the conventional moment of inertia of the cross section.

The typical properties of n and E for the Ludwick-type materials considered in this study are.

- $n = 1$ and $E = 207$ GPa for steel (linear elastic material),
- $n = 2.16$ and $E = 458.5$ MPa for annealed copper,
- $n = 4.785$ and $E = 455.8$ MPa for the NP8 aluminum alloy,

where a linear material such as steel ($n = 1$) can be considered in terms of the GMI I_g.

To apply I_g to column buckling, rectangular and elliptical cross sections were considered in this study. The configurations of each cross-sectional feature with corresponding width and depth dimensions are presented in Fig. 2a and b, respectively.

2.2 Formulation of GMI I_g

2.2.1 Rectangular cross section

GMI I_g was reformulated to consider column buckling. Applying Eq. 5 to the cross section in Fig. 2a yields I_g[3] as

$$I_g = \frac{0.5^{(1+1/n)} n}{2n+1} ab^{2+1/n}. \tag{6}$$

The GMI I_g is initially expressed in terms of a and b, as shown in Eq. 6. For column buckling analysis, it is desirable to express I_g as an area A, rather than in terms of a and b. This is because the magnitude of A differs for different cross-sectional shapes with the same a and b, and it is effective to compare buckling behaviors for the same A. Therefore, the ratio of b to a, which is defined as the aspect ratio α in Fig. 2a, is defined as

$$\alpha = \frac{b}{a}. \tag{7}$$

Then, the area A is expressed as $A = ab$, and a and b are solved for a uniform area A as

$$a = \sqrt{\frac{A}{\alpha}},\ b = \sqrt{\alpha A}. \tag{8}$$

Subsequently, considering Eq. 8, I_g in Eq. 6 is rearranged in terms of n, α, and A as follows:

$$I_g = \frac{0.5^{(1+1/n)}}{2+1/n}\alpha^{n1}A^{n2} = \beta A^{n2},\ \beta = \frac{0.5^{1+1/n}}{2+1/n}\alpha^{n1}, \tag{9}$$

where $n_1 = (1+1/n)/2$ and $n_2 = (3+1/n)/2$. In Eq. 9, β, which is called the GMI coefficient, is dimensionless, where I_g is computed using the given A.

2.2.2 Elliptical cross section

Applying Eq. 5 to the elliptical cross section in Fig. 2b yields I_g as [4]

$$I_g = \frac{2ab^{n+2}}{n+3} \times B\left(\frac{1}{2}, \frac{n+2}{2}\right), \tag{10}$$

where B is a beta function given explicitly in a definite integral form.

Similarly, the aspect ratio α for an elliptical cross section is defined as

$$\alpha = \frac{b}{a}. \tag{11}$$

Then, the area A is expressed as $A = \pi ab/4$, and a and b are solved for a uniform area A as

$$a = 2\sqrt{\frac{A}{\alpha\pi}},\quad b = 2\sqrt{\frac{\alpha A}{\pi}}. \tag{12}$$

Subsequently, considering Eq. 12, the GMI I_g in Eq. 10 is rearranged explicitly in a definite integral form in terms of n, α, and A as

$$I_g = \frac{4\alpha^{n1}A^{n2}}{\pi^{n2}}\int_0^1 \zeta^{2n1}\sqrt{1-\zeta^2}d\zeta = \beta A^{n2},\ \beta = \frac{4\alpha^{n1}}{\pi^{n2}}\int_0^1 \zeta^{2n_1}\sqrt{1-\zeta^2}d\zeta, \tag{13}$$

where the GMI coefficient β can be calculated numerically using the Runge–Kutta method, which is the direct integration method considered in this study.

As indicated in Eqs. 9 and 13, β depends on the cross-sectional shape (rectangular or elliptical), n, and α. Note that I_g has physical dimensions of $I_g = [A]^{n_2} = [L]^{3+1/n}$, as shown in Eqs. (9) and (13). If A is given in cm^2, then the units of I_g are cm^4 with $n = 1$ for steel (the linear material), $cm^{3.463}$ with $n = 2.16$ for annealed copper, and $cm^{3.209}$ with $n = 4.785$ for the NP8 aluminum alloy.

Table 1 Comparison GMI I_g ($A = 15\ cm^2$) between this study and references

Shape	n and α	Dater source	GMI I_g
Rectangular	$n = 2.16, \alpha = 0.3$	This study	$6.63820\ cm^{3.463}$
		Reference [14]	$6.63820\ cm^{3.463}$
	$n = 4.785, \alpha = 0.5$	This study	$9.92946\ cm^{3.209}$
		Reference [14]	$9.92946\ cm^{3.209}$
Elliptical	$n = 2.16, \alpha = 0.7$	This study	$11.7558\ cm^{3.463}$
		References [4, 6]	$11.7543\ cm^{3.463}$
	$n = 4.785, \alpha = 1.0$	This study	$14.4133\ cm^{3.209}$
		References [4, 6]	$14.4121\ cm^{3.209}$

Table 2 Comparison of GMI I_g ($A = 15\ cm^2$) between cross-sectional shapes

n and α	Shape	GMI I_g Ratio	
$n = 1, \alpha = 0.3$	Rectangular	$5.6250\ cm^4$	1.0472
	Elliptical	$5.3715\ cm^4$	–
$n = 2.16, \alpha = 0.5$	Rectangular	$9.6456\ cm^{3.463}$	1.0495
	Elliptical	$9.1910\ cm^{3.463}$	–
$n = 4.785, \alpha = 1$	Rectangular	$15.097\ cm^{3.209}$	1.0475
	Elliptical	$14.413\ cm^{3.209}$	–

2.3 Numerical example of GMI I_g

The GMI coefficient β is computed using Eqs. 9 and 13 for the given values of n and α, and then, the value of I_g is calculated from β using Eqs. 9 and 13 for the given area A of a rectangular or elliptical shape.

Table 1 compares the GMI I_g results from this study to those presented in references [3–6] to verify the reformulation of I_g developed in this study. The two results for I_g obtained by changing the values of α for two typical nonlinear materials ($n = 2.16$ and 4.785 with $A = 15\ cm^2$) are in good agreement, as shown in Table 1, indicating that the reformulation of I_g developed in this study yields correct results.

It is noteworthy to compare the GMI I_g results for rectangular and elliptical cross sections, which are often used for structural members in practical engineering. Table 2 presents a comparison of the three material constants n for the same α and $A(15\ cm^2)$ values. The I_g value of a rectangle is always approximately 5% greater than the I_g value of an ellipse, regardless of the magnitudes of n and α. Note that the ratios of 1.0472, 1.0495, and 1.0475 for given $n = 1, 2.16$, and 4.785 are similar, but not identical. Additionally, although all results are not shown here, the ratio for rectangular to elliptical shapes is always the same, regardless of α.

The GMI coefficient β expressed in Eqs. 9 and 13 depends on the cross-sectional shape, material constant n,

and aspect ratio α. Once a surface map of β is graphically derived by varying n and α, then $I_g = \beta A^{n2}$ in Eqs. 9 and 13 can be easily calculated for a given area A. Surface maps of β are reported for $0 < n \leq 10$ and $0 < \alpha \leq 1.5$ for the rectangle in Fig. 3a and ellipse in Fig. 3b. These surface maps indicate that β increases with increases in n and α. According to these results, the greatest values of β occur at the greatest values of $n = 10$ and $\alpha = 1.5$ in $0 < n \leq 10$ and $0 < \alpha \leq 1.5$. As expected, for cross sections with the same n and α, the β value of the rectangular cross section is always approximately 5% greater than the β value of the elliptical cross section, as indicated in Table 2.

A practical example of calculating the GMI I_g in dimensional units is illustrated in Fig. 4, which presents I_g versus α curves according to the cross-sectional shape with $A = 20$ cm^2. The I_g versus α curves are nonlinear because I_g increases as α increases, indicating that the greater the depth of the cross section, the higher the bending stiffness. When $\alpha = 1$, meaning $a = b$, I_g is the same relative to the w axis and h axis. In Fig. 4a, I_g with $\alpha > 1$ corresponding to the weak axis, whereas I_g with $\alpha < 1$ corresponds to the

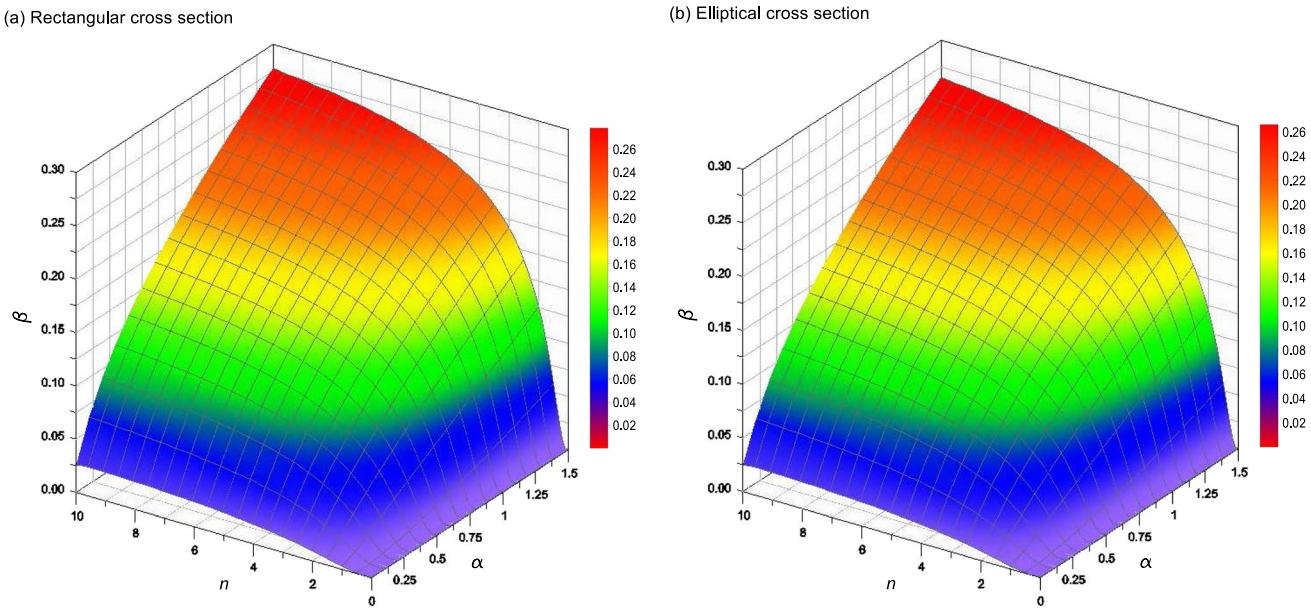

Fig. 3 Surface map β by varying n and α of **a** rectangular and **b** elliptical cross section

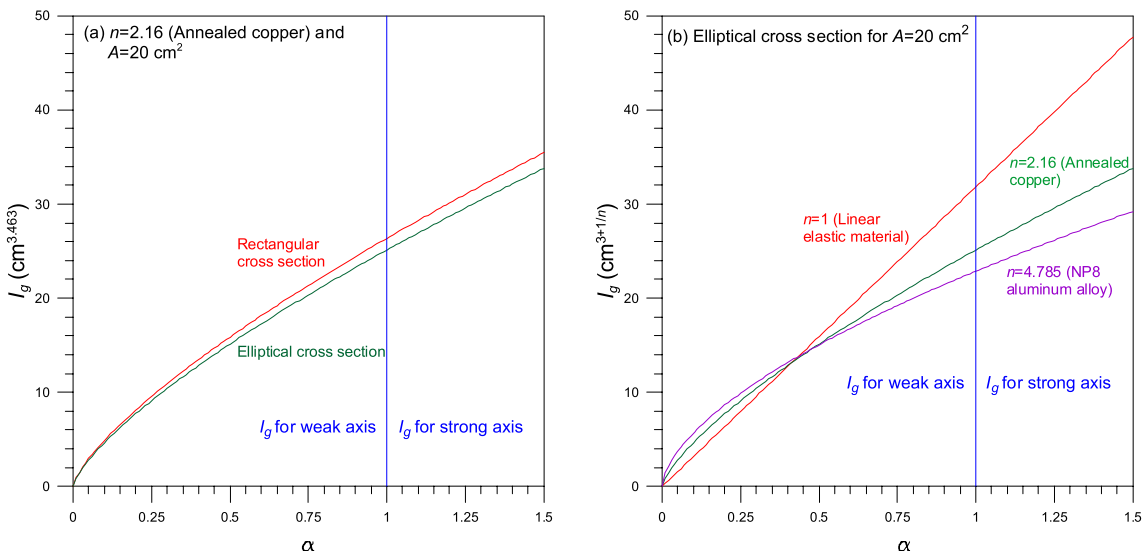

Fig. 4 I_g *I*versus α curves: **a** by cross-sectional shape and **b** by material constant n

strong axis. It is important not to overestimate the buckling load P_{cr}, so it is better not to apply I_g to the strong axis ($\alpha < 1$) when calculating P_{cr}. The I_g value of a rectangular cross section is approximately 5% greater than that of an elliptical cross section. Figure 4b presents I_g versus α curves according to the material constant n with $A = 20\,\text{cm}^2$ for an elliptical cross section, where I_g increases with an increasing α. The I_g versus α curves are nonlinear for $n = 2.16$ and 4.785 (i.e., nonlinear materials), whereas the curve is linear for $n = 1$(i.e., linear material).

3 Application of GMI I_g to buckled column elastica

3.1 Mathematical modeling of column buckling

The GMI I_g was applied to post-buckling column elastica. We present and discuss the mathematical modeling of elastica, numerical solution methods, and numerical experiments. In this study, the buckling loads of a simple column made of Ludwick-type materials were evaluated.

Figure 5a presents a simple support column of length l made of a Ludwick-type material that is loaded with an external load P at the top end, which moves downward after buckling. The column contains no initial imperfections, meaning it is perfectly straight until buckling begins. When P is smaller than the buckling load P_{cr} (i.e., $P < P_{cr}$), the axis of the column represented by the dotted

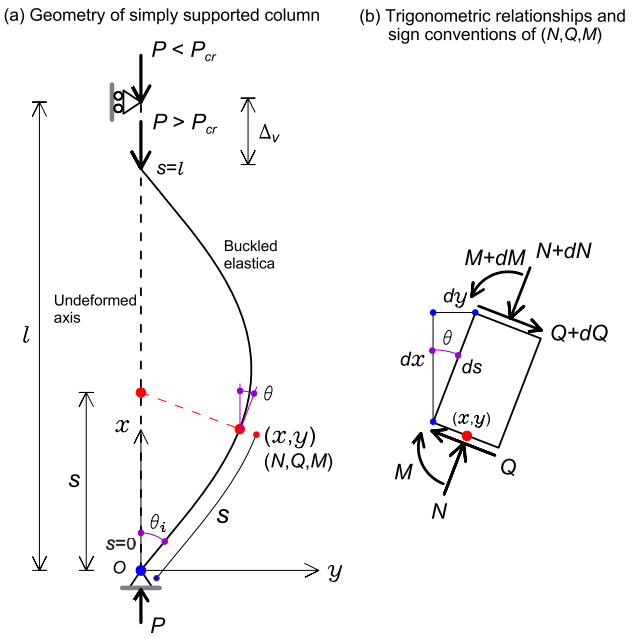

Fig. 5 **a** Geometry of simply supported column and **b** trigonometric relationships of buckled column element and its sign conventions of (N, Q, M)

curve remains a straight line. As P gradually increases and eventually reaches P_{cr} (i.e.,$P = P_{cr}$), the column buckles and elastically deforms. The shape of the highly deformed column after buckling, which is called an elastica, is illustrated by the solid curve in rectangular coordinates (x, y) originating from the base end o. The arc length at (x, y) measured from the base end is displayed in s. Based on the inextensibility/incompressibility of the column, the elastica arc length matches the original length l. At any (x, y), the rotational angle of the cross section is denoted as θ and the vertical deflection at the top end $(s = l)$ is represented by Δ_v. The θ value at the base end $(s = 0)$ is denoted as θ_i. The internal force consists of (N, Q, M) at any (x, y) in Fig. 5, which denotes the axial force, shear force, and bending moment, respectively. Figure 5b presents the trigonometric relationships of a post-buckling column element at coordinates (x, y) and the sign convention of the positive internal forces of (N, Q, M) imposed on the element.

The internal forces of (N, Q, M) at any (x, y) can be expressed using the post-buckling equilibrium state presented in Fig. 5a as follows:

$$N = P\cos\theta, \tag{14}$$

$$Q = P\sin\theta, \tag{15}$$

$$M = Py. \tag{16}$$

The trigonometric relationships of the buckled column element presented in Fig. 5b are based on the Bernoulli–Euler beam theory as follows:

$$\frac{\mathrm{d}x}{\mathrm{d}s} = \cos\theta, \tag{17}$$

$$\frac{\mathrm{d}y}{\mathrm{d}s} = \sin\theta. \tag{18}$$

By using the exact curvature of $\kappa = \mathrm{d}\theta/\mathrm{d}s$ and GMI $I_g\left(= \beta A^{n2}\right)$, the bending moment M can be expressed as follows:

$$M = EI_g\kappa^{1/n} = \beta EA^{n2}\left(\frac{\mathrm{d}\theta}{\mathrm{d}s}\right)^{1/n}. \tag{19}$$

Combining Eqs. 16 and 19, and rearranging in terms of $\mathrm{d}\theta/\mathrm{d}s$ yields

$$\frac{\mathrm{d}\theta}{\mathrm{d}s} = \left(\frac{Py}{\beta EA^{n2}}\right)^{n}. \tag{20}$$

To discuss numerical results in a dimensionless form, dimensionless system parameters are defined as follows:

$$\lambda = \frac{s}{l}, \tag{21}$$

$$\xi = \frac{x}{l}, \tag{22}$$

$$\eta = \frac{y}{l}, \tag{23}$$

$$\delta_{\mathrm{v}} = \frac{\Delta_{\mathrm{v}}}{l}\left(= 1 - \xi_{\lambda=1}\right), \tag{24}$$

$$p = \frac{Pl^{2n1}}{EA^{n2}}, \tag{25}$$

where (λ, ξ, η) are dimensionless coordinates, δ_{v} is the dimensionless vertical deflection at the top moveable end $(s = l)$, and p is the normalized load parameter.

By combining the system parameters in Eqs. 17, 18, and 20, we can derive a dimensionless form of the governing differential equations for a post-buckling column that follows the Ludwick constitutive law as

$$\frac{\mathrm{d}\xi}{\mathrm{d}\lambda} = \cos\theta, \tag{26}$$

$$\frac{\mathrm{d}\eta}{\mathrm{d}\lambda} = \sin\theta, \tag{27}$$

$$\frac{\mathrm{d}\theta}{\mathrm{d}\lambda} = \left(\frac{p\eta}{\beta}\right)^{n}. \tag{28}$$

Considering the boundary conditions for the initial problems in Eqs. 26–28, the coordinates (x, y) of the base end $(s = 0)$ are zero and have the following dimensionless form:

$$\xi = 0, \eta = 0 \text{ at } \lambda = 0 \tag{29}$$

One of the initial boundary conditions, namely the rotation θ_i at the bottom end $(\lambda = 0)$, is not considered as an initial value in the differential Eqs. 26–28 and is derived later through numerical analysis.

At the top end $(s = l)$, the coordinate y is zero, and its dimensionless form is

$$\eta = 0 \text{ at } \lambda = 1 \tag{30}$$

The internal forces (N, Q, M) of a post-buckling column are normalized as follows:

$$\overline{n} = \frac{Nl^{2n1}}{EA^{n2}} = p\cos\theta, \tag{31}$$

$$\overline{q} = \frac{Ql^{2n1}}{EA^{n2}} = p\sin\theta, \tag{32}$$

$$\overline{m} = \frac{Ml^{1/n}}{EA^{n2}} = p\eta. \tag{33}$$

3.2 Numerical solution methods and verification

There are no closed-form solutions for Eqs. 26 and 28. Therefore, to solve these differential equations numerically, approximate numerical methods were developed to compute the buckling loads and post-buckling elastica. The input column parameters were the cross-sectional shape (rectangular or elliptical), span length$l$, cross-sectional dimensions of a and b, material properties of (n, E), and load P. The corresponding dimensionless parameters α, β, and p are calculated using these dimensional parameters. To compute the elastica of (ξ, η), the Runge–Kutta method [25], which is a direct numerical integral method, was used to integrate Eqs. 26–28. To determine the unknown θ_i at the base end $(\lambda = 0)$, a numerical method for solving nonlinear equations, such as the bisection method [25], can be applied. This type of solution method for deriving an unknown θ_i has been frequently used to solve the initial and boundary value problems in the literature [14]. For interested readers, the numerical method for calculating the elastica of (ξ, η, θ) is described below.

(1) Set the column parameters of the cross-sectional shape n, α, and p (and calculate β for the given n and α).
(2) Assume a trial unknown θ_i at $\lambda = 0$. The first trial θ_i is $\theta_i = 0$.
(3) Subject the boundary conditions in Eq. 29 to Eqs. 26 to 28 and integrate Eqs. 26 to 28 at $0 \le \lambda \le 1$ using the Runge–Kutta method. Subsequently, the trial solution (ξ, η, θ) along the arc length λ is obtained.
(4) In this calculation, evaluate $E_{\mathrm{r}} = \eta_{\lambda=1}$ for the boundary condition in Eq. 30 considering the following convergence criterion:

$$\left|E_{\mathrm{r}}\right| \le 1 \times 10^{-8}. \tag{34}$$

If the criterion in Eq. 34 is satisfied, then calculation is stopped after an additional calculation of $(\overline{n}, \overline{q}, \overline{m})$.

5) If the above criterion is not met, then increase the trial θ_i by Δ and return to step 2 with the advanced trial $\theta_i (\leftarrow \theta_i + \Delta)$.

6) Monitor whether the sign of $E_{\mathrm{r1}} \times E_{\mathrm{r2}}$ has changed during steps 2–5, where E_{r1} and E_{r2} are E_{r} values corresponding to the previous and current trials, respectively. If the sign of $E_{r1} \times E_{r2}$ does not change until $\theta = \pi$, then the given p

is smaller than p_{cr} and the column is still straight. Because θ_i cannot exceed π, we stop calculating. Here, the buckling load parameter p_{cr} is defined as

$$p_{\mathrm{cr}} = \frac{P_{\mathrm{cr}} l^{2n1}}{EA^{n2}}. \tag{35}$$

7) When changing the sign of$E_{\mathrm{r1}} \times E_{\mathrm{r2}}$, the target solution for θ_i is between θ_{i_1},E_{r1}, and θ_{i_2} with E_{r1}. A more advanced new trial θ_{i_3} for the target solution θ_i compared to θ_{i_1} and θ_{i_2} is evaluated using the bisection method [25] as

$$\theta_{i3} = \frac{\theta_{i1} + \theta_{i2}}{2}. \tag{36}$$

8) Once the step 7 is completed, repeat the steps above until the following criterion is satisfied:

$$\frac{\theta_{i1} + \theta_{i2}}{2} \le 1 \times 10^{-5}. \tag{37}$$

9) If the criterion in Eq. 37 is satisfied, compute $(\overline{n}, \overline{q}, \overline{m})$ and stop the calculation. If the sign of $E_{r1} \times E_{r2}$ for a given p in the steps above does not change until $\theta_i = \pi$, then the given p is less than p_{cr}, meaning the column does not buckle, as mentioned in step 6.

A numerical solution method for calculating the buckling load parameter p_{cr} was developed based on the fact that the buckling loads p_{cr} for nonlinear columns following the Ludwick constitutive law are jump buckling loads [5]. A column under a load parameter $p < p_{\mathrm{cr}}$ does not buckle, meaning $\theta_i = 0$, whereas a column with $p > p_{\mathrm{cr}}$ buckles, meaning $\theta_i \neq 0$. Therefore, it is clear that p will be p_{cr}, which is the smallest p that θ_i has encountered. A numerical method for calculating p_{cr} can be developed in the same manner by adopting the numerical method for a buckled column described above. Starting with $p = 0$, we increase p by the increment $\Delta p (< \pi)$ and steps 2–5 are performed until $E_{\mathrm{r1}} \times E_{\mathrm{r2}}$ changes its sign. Δp can be arbitrarily selected from $0 < \Delta p < \pi$. Then, p_{cr} is located between two adjacent p_a and p_b, between which the previous sign of $E_{\mathrm{r1}} \times E_{\mathrm{r2}}$ does not change, and the current sign of $E_{\mathrm{r1}} \times E_{\mathrm{r2}}$ changes. In this calculation, p_{a} is p_2 from the previous iteration, whereas p_{b} is p_1 from the current iteration. Therefore, $p_{\mathrm{b}} > p_{\mathrm{a}}$. Steps 2–5 are iterated from p_{a}–p_{b} in small increments $\Delta p \left(< p_{\mathrm{b}} - p_{\mathrm{a}}\right)$ until the following convergence criterion is satisfied:

$$p_{\mathrm{cr}} \approx p_{\mathrm{b}}, \text{ if } D = \frac{p_{\mathrm{b}} - p_{\mathrm{a}}}{p_{\mathrm{b}}} \le 1 \times 10^{-5}. \tag{38}$$

Figure 6 presents a typical example of determining p_{cr} for a rectangular cross section with $n = 2.16$ and $\alpha = 0.5$. In the first iteration with $i = 1$, p_{b} for $\Delta p = 0.1$ is $p_{\mathrm{b}} = 0.6$ with $D = (0.6 - 0.5)/0.1 = 1 > 1 \times 10^{-5}$, where the sign of $E_{\mathrm{r1}} \times E_{\mathrm{r2}}$ changes, implying that the solution

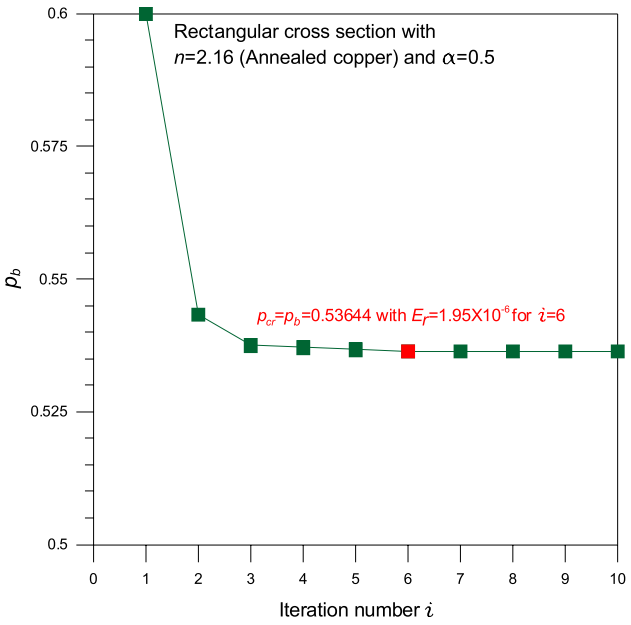

Fig. 6 Convergence analysis according to iteration number i to obtain buckling load parameter p_{cr}

p_{cr} lies within $0.5 \left(= p_{\mathrm{a}}\right) < p_{\mathrm{cr}} < 0.6 \left(= p_{\mathrm{b}}\right)$. Finally, for $i = 6$, p_{cr} is determined as $p_{\mathrm{cr}} \left(= p_{\mathrm{b}}\right) = 0.53644$ with $E_{\mathrm{r}} = 1.95 \times 10^{-6} < 1 \times 10^{-5}$.

To calculate the buckling load parameter p_{cr} and buckling elastica (ξ, η, θ) using the analytical and numerical methods described above, two FORTRAN programs were designed. These programs contain a subroutine that calculates the GMI I_{g}. For validation purposes, a comparison of the buckling load P_{cr} values calculated in this study and the reference values for steel columns ($n = 1$ and $E = 270$ GPa) for $l = 1$ m and $A = 20$ cm^2 are presented in Table 3. The references presented here are the only results published in the literature. Although the P_{cr} value in this study was approximated using numerical methods, it matches well with the closed solution from reference [24] (within five digits of accuracy).

3.3 Numerical experiments

Numerical experiments were conducted for the buckling load parameter p_{cr} and elastica (ξ, η) using the FORTRAN programs developed in this study. As discussed in Sect. 2.1, three different material constants were considered in our numerical experiments: $n = 4.785$ for the NP8 aluminum alloy, $n = 2.16$ for annealed copper, and $n = 1$ for steel. In our numerical experiments, only the fundamental critical buckling load parameters p_{cr} of the columns were calculated because a higher buckling load is less important than the critical p_{cr} [26]. Therefore, only the post-buckling equilibrium paths versus p_{cr} are presented.

Table 3 Comparisons* of buckling load P_{cr} between this study and reference

Shape	α	Width a (cm)	Depth b (cm)	Buckling load P_{cr}(kN)	
				This study	Reference [24]
Rectangular	0.3	8.165	2.449	204.30	204.30
	0.5	6.325	3.162	340.50	340.50
Elliptical	0.7	6.031	4.222	455.22	455.22
	1.0	5.046	5.046	650.31	650.31

*$l = 1$ m, $A = 20$ cm^2 and $E = 207$ GPa for steel column ($n = 1$)

Table 4 Comparisons* of buckling load P_{cr} between cross-sectional shapes

n, α and E**	Shape P_{cr} (kN)	(kN)) ratio	
$n = 1, \alpha = 0.3,$	Rectangular	204.30	1.0472
$E = 207$GPa	Elliptical	195.09	–
$n = 2.16, \alpha = 0.5,$	Rectangular	5.2197	1.0495
$E = 458.5$MPa	Elliptical	4.9737	–
$n = 4.785, \alpha = 1,$	Rectangular	15.851	1.0475
$E = 455.8$MPa	Elliptical	15.132	–

*$l = 1$ m and $A = 20$ cm^2

**See Sect. 2.1 for n and E of Ludwick-type material

It is relevant to compare the buckling loads p_{cr} between rectangular and elliptical cross sections, which are often used for structural members in practical engineering. Table 4 presents comparisons of p_{cr} values for three different values of n with the same α, l(= 1 m), and A(= 20 cm^2). The p_{cr} value of the rectangular section is always approximately 5% greater than that of the elliptical section, regardless of the magnitudes of n and α. It is noteworthy that the ratios in this table are the same as those in Table 2, where the GMI I_g values are compared. Additionally, even for values not shown here, the ratios of values for rectangular to elliptical cross sections are always the same, regardless of α.

We now discuss the various effects of the dimensionless system parameters on the buckling load parameter p_{cr}. Figure 7a presents the p_{cr} versus aspect ratio α curves obtained by varying the material constant n. As expected, p_{cr} increases with an increase in α because a larger α results in a larger I_g for the cross section. The buckling load parameter p_{cr} curves for nonlinear materials with $n = 4.785$ and $n = 2.16$ are nonlinear, whereas the p_{cr} curve for the linear material with $n = 1$ is linear. One can see that the order of the magnitudes of p_{cr} values for columns with three different n values depends on α. For example, the magnitude order for $\alpha = 0.5$ is from $n = 2.16$ to $n = 4.785$ to $n = 1$, whereas the orders for $\alpha = 0.1$ and 0.9 differ from the order for $\alpha = 0.5$. The buckling load p_{cr} in dimensional units for an elliptical column with $l = 1$ m and $A = 20$ cm^2 with a varying α is presented in Fig. 7b. Here, the conversion from the dimensionless p_{cr} to the dimensional buckling load P_{cr} was calculated using Eq. 35 as $P_{cr} = \left(EA^{n2}/l^{2n1}\right)p_{cr}$. p_{cr} increases with an

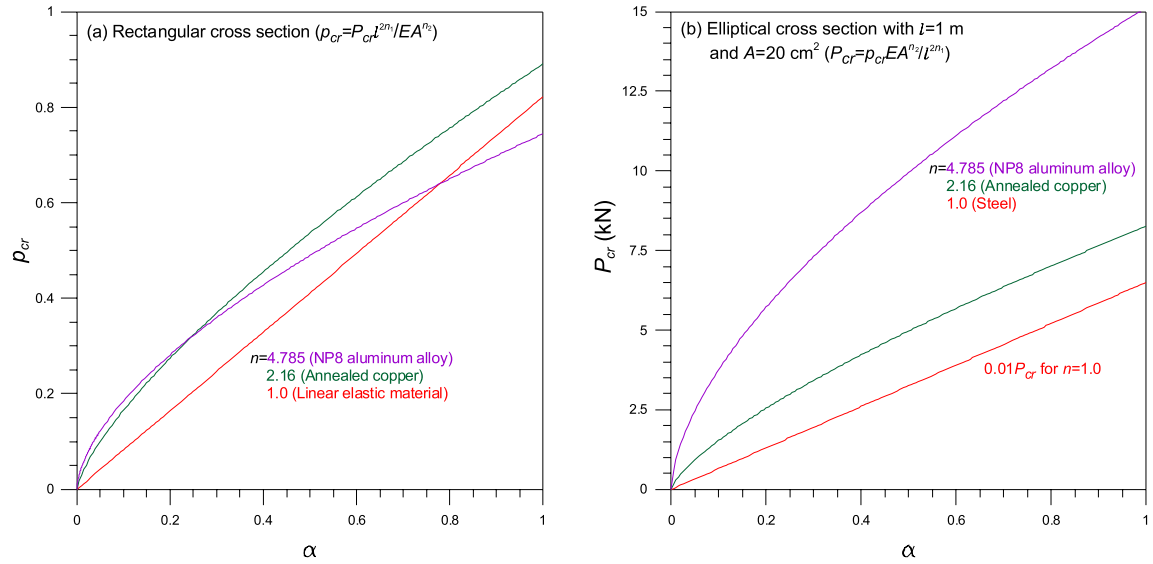

Fig. 7 Buckling curves of **a** dimensionless p_{cr} and **b** dimensional p_{cr} by changing α

increase in α, similar to Fig. 7a. The increasing slope of p_{cr} is steeper at smaller α values. The dimensionless p_{cr} does not exhibit large deviations between the three different columns, whereas the dimensional p_{cr} exhibits large deviations. This is because p_{cr} is related to the Young's modulus E, as shown in Eq. (35), which exhibits large deviations for the three different materials. As a result, the corresponding p_{cr} is highly dependent on E, even if the non-dimensional p_{cr} does not vary significantly among the three different materials.

For nonlinear elastic members, the slenderness ratio s_r can be expressed as

$$s_r = \frac{l}{\sqrt{I_g/A^z}}, \tag{39.1}$$

where z is an exponential constant, so s_r is dimensionless. Then, z is derived such that $z = n_1$ and s_r is finally expressed as

$$s_r = \frac{l}{\sqrt{I_g/A^{n1}}} = \frac{l}{\sqrt{\beta A}}. \tag{39.2}$$

The area A and length l are expressed in terms of s_r for a given β as

$$A = \frac{l^2}{\beta s_r^2},\ l = s_r\sqrt{\beta A}. \tag{40}$$

To visualize the effects s_r on the buckling load P_{cr}, P_{cr} versus s_r curves are presented for two cases. Figure 8a presents the curves with a varying A and Fig. 8b presents the curves with a varying l according to Eq. 40. The remaining column parameters are also presented in this figure. As expected, as s_r increases, P_{cr} decreases, exhibiting a very large decreasing rate. For example, when comparing $P_{cr} = 21.33$ kN with $s_r = 50$ and $P_{cr} = 0.1754$ kN to $s_r = 200$ for $n = 2.16$ in Fig. 8a, the difference is 121.6 (=21.33/0.1754) times, which is relatively large. This indicates that s_r is one of the most important factors for column design.

It is important to gain a complete understanding of the load parameter $p(> p_{cr})$ versus (δ_v, θ_i) curve, which is called the equilibrium path. Figure 9 presents the equilibrium paths of rectangular cross sections with $\alpha = 0.5$ for three different materials. The equilibrium paths with respect to δ_v are presented in Fig. 9a. For $n = 2.16$, if $p < 0.5364(= p_{cr})$, then δ_v does not deform and the column does not buckle. However, as p gradually increases and eventually reaches $p_{cr} = 0.5364$, δ_v abruptly increases from $\delta_v = 0$ to $\delta_v = 0.4813$, causing fatal buckling of the column with unexpected and dangerous consequences. When the column buckles, there are possible two equilibrium paths: the unstable path indicated by the dashed line and stable path indicated by the solid line. The column only follows the unstable path, which is a pass-through path, from its initial straight state until it reaches the final steady equilibrium state of the post-buckling column (see Fig. 10b). As described previously, in the solution method for calculating p_{cr}, the unstable and stable paths meet at p_{cr}, resulting in a sudden jump from $\delta_v = 0$ in the initially straight state to $\delta_{v,pcr} = 0.4813$ in the buckled state. The unstable path is strongly nonlinear and δ_v decreases as p_{cr} increases. Additionally, the stable path is also strongly nonlinear and as p_{cr} increases, δ_v increases, approaching the maximum physical value of a simple column at $\delta_v = 2$. For a linear elastic column with $n = 1$ (e.g., steel), the column remains straight until buckling at $p = 0.4112(= p_{cr})$,

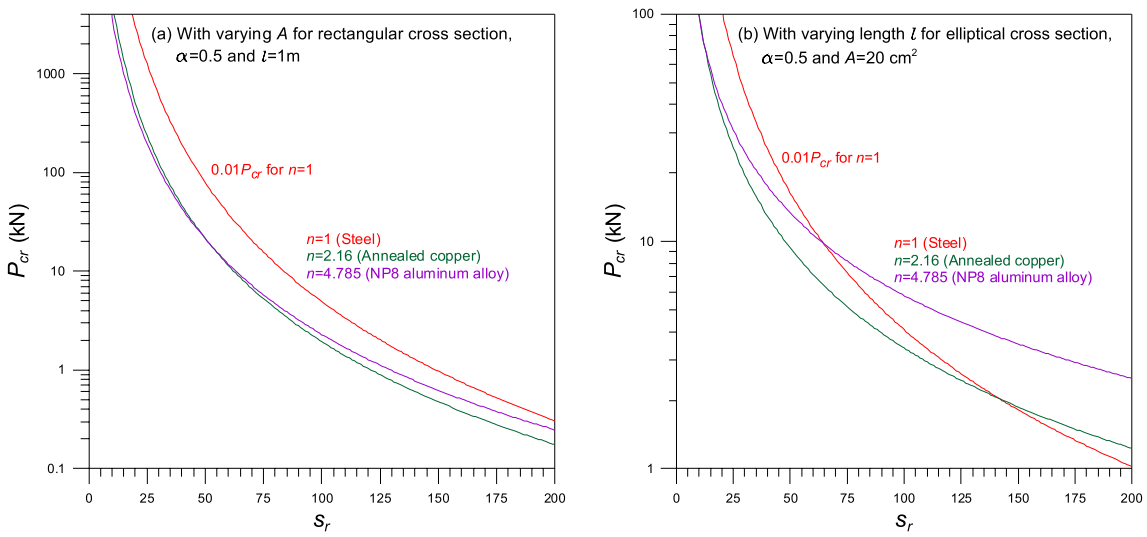

Fig. 8 s_r versus P_{cr} curves: **a** with changing A for rectangular cross section and **b** with changing l for elliptical cross section

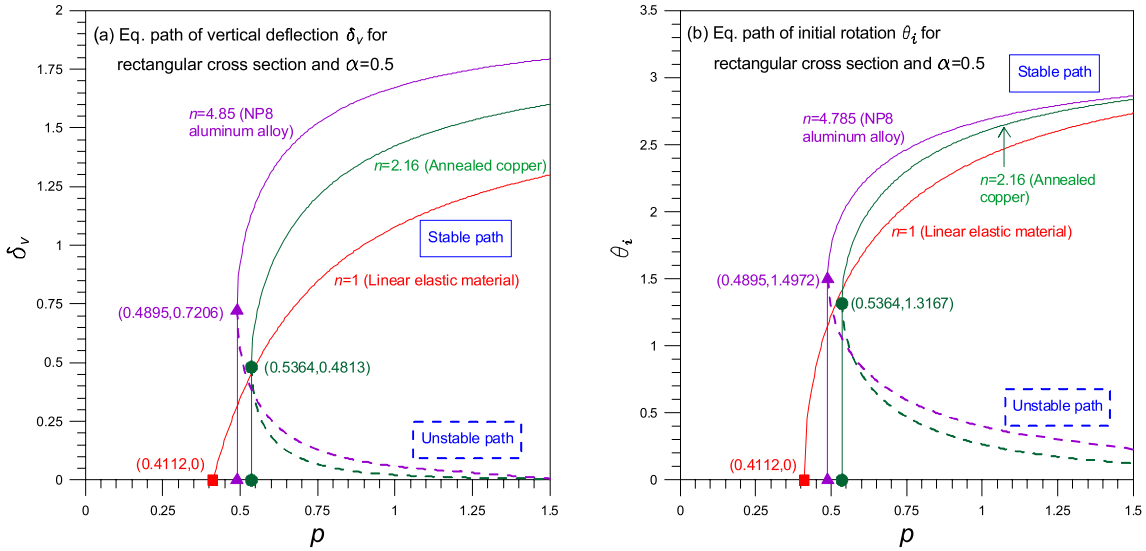

Fig. 9 Equilibrium paths for rectangular cross section: **a** vertical deflection δ_v and **b** initial rotation θ_i

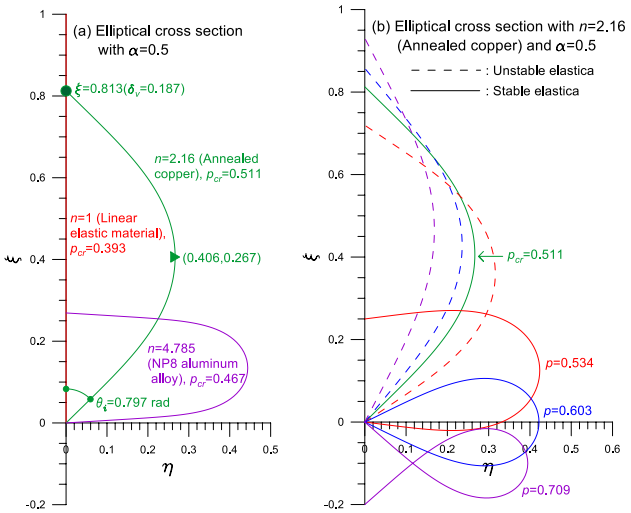

Fig. 10 Elastica for elliptical cross section: **a** buckling elastica by n and **b** post-buckled column elastica for $n = 2.16$ with a varying p

meaning there is no unstable path and δ_v does not abruptly jump, unlike the nonlinear materials with $n = 2.16$ and $n = 4.785$. Therefore, for linear columns, buckling can be detected immediately after it occurs, facilitating the avoidance of catastrophic collapse caused by buckling. After buckling with a stable path, the equilibrium path is strongly nonlinear, where δ_v increases with an increasing p. The equilibrium paths of the initial rotation θ_i are presented in Fig. 9b. These paths are also nonlinear, similar to the equilibrium path for δ_v, where θ_i increases as p increases and eventually approaches $\theta_i = \pi$.

In practical engineering fields, it is necessary to understand the elastica behavior of buckling and post-buckling processes for column design. In Fig. 10a, for the elliptical cross section, the buckling elastica (ξ, η) of the steel $(n = 1)$, annealed copper $(n = 2.16)$, and NP8 aluminum alloy $(n = 4.785)$ columns with $\alpha = 0.5$ are presented. The larger the value of n, the more severe the elastica. For $n = 1$, the column remains straight at the buckling load $p_{cr} = 0.393$, whereas for $n = 2.16$ and 4.785, the buckling elastica deforms significantly, which corresponds to the equilibrium paths shown in Fig. 9. For $n = 2.16$, a very large vertical deflection of $\delta_v = 0.187(= 1 - 0.813)$ occurs at $p_{cr} = 0.51$, which is denoted by, leading to abrupt deformation immediately after column buckling. Because these sharp deformations of buckling elastica are unpredictable and cause catastrophic collapse, it is critical to exercise caution when determining p_{cr} in nonlinear column design. The post-buckling elastica of the elliptical cross section for $\alpha = 0.5$ and $n = 2.16$ is presented in Fig. 10b, where four elastica with $p = 0.709, 0.603, 0.534$, and $0.511\left(= p_{cr}\right)$ are included. The dashed elastica with $p\left(> p_{cr}\right) = 0.709, 0.603$, and 0.534 is unstable before the bucking elastica for $p_{cr} = 0.511$ occurs. An unstable dashed elastica represents a path that cannot exist naturally. In the unstable region before the buckling elastica, an elastica with $p(> p_{cr})$ is present in the upper region close to the unbuckled straight column and all elastica with $p > p_{cr}(= 0.511)$ exist in this upper region. As discussed above, the top end of the column catastrophically moves to the deformation coordinates (0.406, 0.267), which are indicated by ▶ in Fig. 10a, immediately after column buckling. After passing through the unstable elastica, the post-buckling elastica, which are indicated by the solid line, becomes stable. In this lower stable region, four buckled elastica with $p = 0.511\left(= p_{cr}\right), 0.534, 0.603$, and 0.709 can be observed. Here, the top end of the elastica with $p > 0.603$ can theoretically be located below the base end because the vertical

deflection δ_v becomes $\delta_v = 1$ when $p = 0.603$. For example, see the elastica with $p = 0.709 (> 0.603)$.

Next, we discuss the internal forces (N, Q, M), and distributed strain ε and stress σ of buckled columns. The dimensionless forms of $(\overline{n}, \overline{q}, \overline{m})$ can be converted into the dimensional form of (N, Q, M) using Eqs. 31–33. For example, a diagram of (N, Q, M) with $n = 4.785$ and $E = 455.8$ MPa for the NP8 aluminum alloy is presented in Fig. 11, where the input parameter areas are the elliptical cross section, $l = 1$ m, $a = 5.642$ cm, and $b = 4.514$ cm ($\alpha = 0.8, A = 20$ cm^2, and $I_g = 19.98$ cm$^{3.209}$). Based on these column parameters, the buckling load, P_{cr}, is calculated as $P_{cr} = 13.223$ kN. As expected, at the mid-arc of the elastica (i.e., $s = 0.5$ m), N_m is $N_m (= P_{cr}) = 13.223$ kN and $Q_m = 0$ because $\theta_m = 0$. At the base end ($s = 0$), N_o is $N_o = 0.667$ kN and $Q_o = 13.206$ kN with $\theta_i = 1.621$ rad, where $P_{cr} (= 13.223\text{kN}) = \sqrt{N_o^2 + Q_o^2}$. Additionally, as expected, at the mid-arc, M_m with $y_{s=0.5m} = 0.445$ m is the maximum value because $M_m = P_{cr} \times y_{s=0.5m} = 5.882$ kNm.

Finally, the distribution of (ε, σ) for the buckling elastica at the mid-arc ($s = 0.5$m), where the maximum bending moment M_m occurs, is presented in Fig. 12. The input column parameters are the same as those in Fig. 11. Given N and M, the distribution of (ε, σ) along the cross-sectional depth h can be obtained as follows:

$$\varepsilon = \varepsilon_N + \varepsilon_M = \left(\frac{|N|}{EA}\right)^n \pm \left(\frac{|M|}{EI_g}\right)^n h, -\frac{b}{2} \le h \le \frac{b}{2}, \quad (41)$$

$$\sigma = E\varepsilon^{1/n}. \quad (42)$$

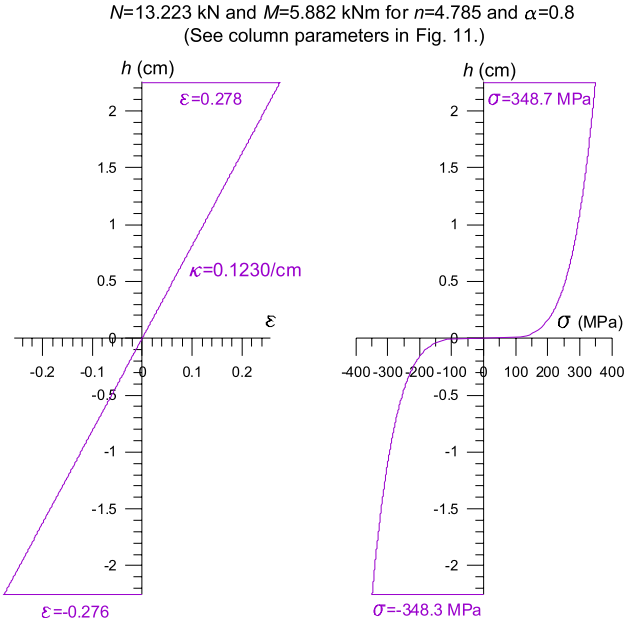

Fig. 12 Buckling strain ε and stress σ at mid-arc for elliptical cross section

For the values of $N_m = 13.223$ kN and $M_m = 5.882$ kNm at the mid-arc in Fig. 11, the corresponding $(\varepsilon_N, \varepsilon_M)$ can be obtained as $\varepsilon_N = +1.596 \times 10^{-9}$ and $\varepsilon_{M,h=\pm b/2} = \pm 0.278$, from which $\varepsilon = +0.278$ and $\varepsilon = -0.276$ at the two edges with $h = \pm b/2$ ($b = 4.514$) were obtained using Eq. 41. Note that $\varepsilon_N = +1.596 \times 10^{-9}$ is very small and almost negligible compared to $\varepsilon_{M,h=\pm b/2}$, and ε is nearly equal to ε_M, implying that the change in the neutral axis position caused

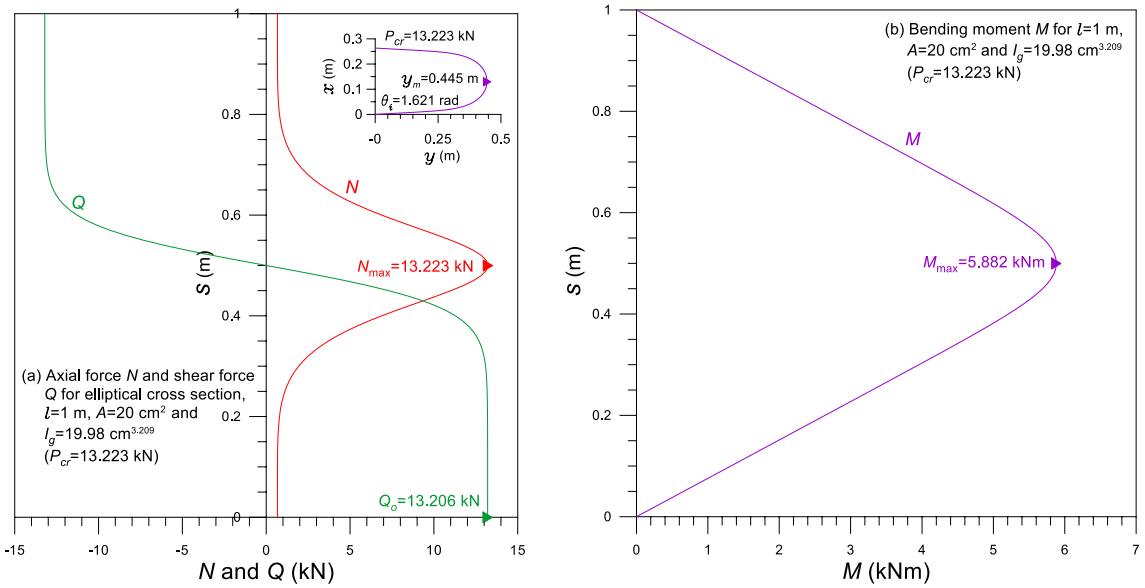

Fig. 11 Buckling internal forces (N, Q, M) for elliptical cross section with $n = 4.785$ and $\alpha = 0.8$

by ε_N is negligible. Considering the values of $\varepsilon = +0.278$ and $\varepsilon = -0.276$ at the two edges, the linear relationship of $\varepsilon = \kappa h$ can be plotted, as shown in Fig. 12, where the curvature of $\kappa = 0.123/\text{cm}$ was calculated using Eq. 19. The nonlinear stress equation $\sigma = E\varepsilon^{1/n}$ was obtained and the result is presented in Fig. 12. The σ_{max} values at the two edges were calculated as $\sigma_{max} = +348.7$ MPa at the top edge and $\sigma_{max} = -348.3$ MPa at the bottom edge. Because the shape of the nonlinearly distributed stress is almost rectangular, it is more advantageous to use the total cross-sectional area for the stress σ compared to the case of linear materials. As shown in Fig. 12, this is beneficial for ensuring column safety when designing nonlinear elastic columns.

4 Concluding remarks

This study investigated the geometric and material nonlinear buckling of simple columns made of Ludwick-type materials. Before modeling nonlinear column buckling, a GMI I_g calculation method was derived based on theories from the open literature and reformulated for rectangular and elliptical cross sections. The buckling of a simple column was considered to apply the reformulated I_g to bending analysis. Nonlinear differential equations that govern the buckled column elastica were derived and numerically solved to obtain the buckling load and elastica of the column. An iterative numerical method was developed to calculate the elastica, where the Runge–Kutta method was used to integrate the governing equations and the bisection method was used to determine the rotational angle at the bottom hinged end. Numerical parametric experiments on GMI I_g for rectangular and elliptical cross sections were discussed in detail. As a major focus of this study, parametric studies on buckling behavior, including buckling load, equilibrium path, buckling and buckled elastica, and the strain and stress distribution of a buckled column, were conducted and discussed in detail. The buckling loads of materials and geometric nonlinear simple columns were reported for the first time in this paper. Additionally, a slenderness ratio applicable to nonlinear elastic members was derived and applied to the buckling problem. The results of this study should be useful for buckling analysis and nonlinear elastic column design. Further studies on the GMI I_g for asymmetric cross-sectional shapes are required, as are further studies on support conditions other than the simply supported columns considered in this study.

Funding The first author acknowledges the support of the National Research Foundation of Korea (Grant number NRF-2020R1C1C1005374).

Declarations

Conflict of interest The authors declare that they have no conflict of interest.

References

1. Mihai LA, Goriely A (2017) How to characterize a nonlinear elastic material?—A review on nonlinear constitutive parameters in isotropic finite elasticity. Proc R Soc A 473:20170607
2. Lewis G, Monasa F (1982) Large deflections of cantilever beams of nonlinear materials of the Ludwick type subjected to an end moment. Int J Nonlinear Mech 17(1):1–6
3. Lee K (2002) Large deflections of cantilever beams of nonlinear elastic material under a combined loading. Int J Nonlinear Mech 37(3):439–443
4. Brojan M, Kosel F (2011) Approximative formula for post-buckling analysis of nonlinearly elastic columns with superellipsoidal cross-sections. J Reinf Plast Comp 30(5):409–415
5. Lee JK, Lee BK (2019) Generalized second moment of areas of regular polygons for Ludwick type material and its application to cantilever column buckling. Int J Struct Stab Dy 19(2):1950010
6. Kim GS, Lee JK, Lee TE, Lee BK (2022) Buckling behavior of nonlinear elastic cantilever column with an elliptical cross—section. Arab J Sci Eng 47:4545–4557
7. Brojan M, Sitar M, Kosel F (2012) On static stability of nonlinearly elastic Euler's columns obeying the modified Ludwick's law. Int J Struct Stab Dy 12(6):1250077
8. Euler L (1774) Methodus inveniendi lineas curvas maximi minimive proprietate gaudentes, sive solutio problematis isoperimetrici latissimo sensu accepti. Lausanne: Apud Marcum Michaelem Bousquet & Socio
9. Bisshopp KE, Drucker DC (1945) Large deflections of cantilever beams. Q Appl Math 3:272–275
10. Aristizabal-Ochoa JD (2007) Large deflection and post-buckling behavior of Timoshenko beam-columns with semi-rigid connections including shear and axial effects. Eng Struct 29(6):991–1003
11. Lee JK, Lee BK (2017) Large defections and buckling loads of cantilever columns with constant volume. Int J Struct Stab Dy 17(8):1750091
12. Oden JT, Childs SB (1970) Finite deflections of a nonlinearly elastic bar. J Appl Mech 37:48–52
13. Lee BK, Wilson JF, Oh SJ (1993) Elastica of cantilevered beam with variable cross-section. Int J Nonlinear Mech 28(5):579–589
14. Lee BK, Oh SJ (2000) Elastica and buckling load of simple tapered columns with constant volume. Int J Solid Struct 37(18):2507–2518
15. Berkey DE, Freedman MI (1978) A perturbation method applied to the buckling of a compressed elastica. J Comput Appl Math 4(3):213–220
16. Giardina RJ, Wei D (2020) Ramberg-Osgood material behavior expression and large deflection of Euler beam. Mathe Mech Solid 26(2):179–198
17. Anatolyevich BP, Yokovlevna GN (2019) Generalized of the Ramberg-Osgood model for elastoplastic materials. J Mater Eng Perform 28:7342–7346
18. Eren I (2013) Analyses of large defections of simply supported nonlinear beams for various arc length functions. Arab J Sci Eng 3(4):947–952
19. Eren I (2008) Determining large defections in rectangular combined loaded cantilever beams made of nonlinear Ludwick type material by means of different arc length assumptions. Sadhana 33(1):45–55

20. Jung JH, Kang TJ (2005) Large deflection analysis of fibers with nonlinear elastic properties. Text Res J 75(10):715–723
21. Saetiew W, Chucheepsakul S (2012) Post-buckling of linearly tapered column made of nonlinear elastic materials obeying the generalized Ludwick constitutive law. Int J Mech Sci 6(1):83–96
22. Borboni A, Santis D (2014) Large deflection of a non-linear, elastic, asymmetric Ludwick cantilever beam subjected to horizontal force, vertical force and bending torque at the free end. Meccanica 49:1327–1336
23. Liu H, Han Y, Yang JL (2017) Large defection of curved elastic beams made of Ludwick type material. Appl Math Mech 38(7):909–920
24. Gere M (2004) Mechanics of materials. Brooks/cole–thomson learning, Belmont, CA, USA
25. Burden RL, Faires DJ, Burden AM (2016) Numerical analysis. Cengage Learning, Boston, MA, USA
26. Carpinteri A, Malvano R, Manuello A, Piana G (2014) Fundamental frequency evolution in slender beams subjected to imposed axial displacements. J Sound Vib 333:2390–2403